

CHARACTERISTICS OF SPIRAL ARMS IN LATE-TYPE GALAXIES

Z. N. HONIG AND M. J. REID

Harvard-Smithsonian Center for Astrophysics, 60 Garden Street, Cambridge, MA 02138, USA; mreid@cfa.harvard.edu

Received 2014 October 2; accepted 2014 December 5; published 2015 February 9

ABSTRACT

We have measured the positions of large numbers of H II regions in four nearly face-on, late-type, spiral galaxies: NGC 628 (M74), NGC 1232, NGC 3184, and NGC 5194 (M51). Fitting log-periodic spiral models to segments of each arm yields local estimates of spiral pitch angle and arm width. While pitch angles vary considerably along individual arms, among arms within a galaxy, and among galaxies, we find no systematic trend with galactocentric distance. We estimate the widths of the arm segments from the scatter in the distances of the H II regions from the spiral model. All major arms in these galaxies show spiral arm width increasing with distance from the galactic center, similar to the trend seen in the Milky Way. However, in the outermost parts of the galaxies, where massive star formation declines, some arms reverse this trend and narrow. We find that spiral arms often appear to be composed of segments of ~ 5 kpc length, which join to form kinks and abrupt changes in pitch angle and arm width; these characteristics are consistent with properties seen in the large N -body simulations of D’Onghia et al. and others.

Key words: galaxies: individual (M51, M74, NGC 1232, NGC 3184) – galaxies: spiral

Supporting material: data behind figures

1. INTRODUCTION

Spiral structures in galaxies have been extensively studied, including the nature and number of arms and values for pitch angles, which measure how tightly wound are the spirals. One characteristic of spirals that has received little attention is the width of arms. For the Milky Way, recent measurements of parallax of molecular masers associated with newly formed massive stars have indicated that the widths of spiral arms, estimated from the scatter of these sources about a segment of a spiral arm, increases with Galactocentric distance (Reid et al. 2014).

Assuming that the Milky Way is not atypical among spiral galaxies, one might expect a similar increase in arm width with radius in other late-type spirals. Whereas the measurement of arm width for the Milky Way is difficult, owing to our location within the Galactic disk and the difficulty of obtaining accurate distance measurements at characteristic distances from the Sun of ~ 5 kpc, it should be straight-forward in external galaxies. Thus, we undertook a detailed study of the patterns of giant H II regions in four nearby, nearly face-on, late-type galaxies that display clear spiral structure.

We use the locations of giant H II regions as tracers of spiral structure. The galaxy images used for measurement of the locations of H II regions are documented in Section 2, along with the methods used to determine positions. Our approach to fitting segments of spiral patterns to these data is presented in Section 3. The results for each galaxy are given in Section 4. Finally, in Section 5, we discuss the characteristics of the spiral arms and compare these characteristics to those of the Milky Way.

2. MEASURED POSITIONS OF H II REGIONS

Table 1 lists information about the images of the four galaxies studied in this paper. All of the images are publicly available on the internet, and we selected high resolution images in H α or blue-filtered emission to maximize the contrast of H II regions with respect to the background continuum emission

from the galaxy. Images were either downloaded in the Flexible Image Transport System (FITS) format or were converted to that format using the ImageMagick program “convert” available at <http://www.imagemagick.org>. We also used this software to prepare images for display in our figures.

FITS format images were loaded into the National Radio Astronomy Observatory’s¹ Astronomical Image Processing System (AIPS). We used the task JMFIT to estimate positions by fitting two-dimensional elliptical Gaussian brightness distributions to individual sub-regions within an image that each contained one H II region. Foreground stars in the Milky Way were easily recognized as point-like objects, usually with diffraction spikes, and excluded. Contamination of our H II region sample by other objects (e.g., supernova remnants or planetary nebulae) should not be significant for these H α or blue-filtered images.

Fitted positions were obtained in pixel units, and we used the pixel scale and assumed galaxy distance given in Table 1 to translate these to physical scales in kiloparsec units. Note that we often adjusted the image display transfer functions when preparing sub-regions of a galaxy for measurement, and that many H II regions are not visible on the low dynamic-range figures published in this paper. We also measured the position of the bright center of each galaxy and subtracted this position from each H II region position in order to translate to galactocentric coordinates. We made no attempt to deproject the H II region positions for these galaxies, which are within about 30° from a face-on orientation. The galactic positions for all H II regions are available.

3. FITTING SPIRAL ARM SEGMENTS

We fit segments of spiral arms to the positions of H II regions using a Bayesian Markov chain Monte Carlo technique. The adopted model is a log-periodic spiral given by

$$R = R_{\text{ref}} e^{-(\beta - \beta_{\text{ref}}) \tan \psi}, \quad (1)$$

¹ The National Radio Astronomy Observatory is a facility of the National Science Foundation operated under cooperative agreement by Associated Universities, Inc.

Table 1
Galaxy Images

| Galaxy | Alias | Type | Distance (Mpc) | Telescope | Filter | Pixel Scale (arcsec) | Reference/Source |
|----------|-------|-----------|----------------|------------|------------|----------------------|------------------|
| NGC 628 | M74 | SA(s)c | 10.0 | <i>HST</i> | H α | 0.150 | 1 |
| NGC 1232 | | SAB(rs)c | 21.0 | VLT | Blue | 0.041 | 2 |
| NGC 3184 | | SAB(rs)cd | 8.2 | JKT | H α | 0.243 | 3 |
| NGC 5194 | M51 | SA(s)bc | 9.4 | <i>HST</i> | H α | 0.050 | 4 |

Notes. Assumed distances used to convert pixel to linear scales. Telescopes: *HST*: Hubble Space Telescope; VLT: Very Large Telescope; JKT: Jacobus Kapteyn Telescope.

References. (1) http://heritage.stsci.edu/2007/41/fast_facts.html; (2) <https://www.eso.org/public/usa/images/eso9845d>; (3) <http://cdsarc.u-strasbg.fr/viz-bin/qcat?J/A+A/426/1135>, Knapen et al. (2004); (4) <http://archive.stsci.edu/prepds/m51/datalist.html>.

where β is galactocentric azimuth defined as zero toward the north and increasing east of north, R_{ref} is the galactocentric radius at azimuth β_{ref} , and ψ is the spiral pitch angle. The parameter β_{ref} was assigned the average of the measured H II region azimuths, leaving two parameters to be solved for: R_{ref} and ψ .

Since the precision in measuring an H II region position ($\lesssim 30$ pc) is significantly better than the intrinsic scatter in their positions about a best-fit spiral segment ($\gtrsim 100$ pc), we also solved for an arm-width parameter (σ_w) to characterize the scatter and to allow for this source of astrophysical noise when fitting a spiral. (While there can be many definitions of arm width, throughout this paper we adopt a Gaussian (1σ) approximation to the distribution of the minimum distances of H II regions from the model arm segment.) We calculated likelihood functions from the weighted residuals, $r_i = \Delta d_i / \sigma_w$, where Δd_i is the minimum distance of the i th H II region from the model spiral (evaluated numerically) and σ_w is its “uncertainty” owing to intrinsic scatter within the arm.

We randomly generated trials (Markov chains) of the two parameters characterizing the spiral arm segment (R_{ref} and ψ) and the parameter characterizing the width of the spiral arm (σ_w) and accepted/rejected these trials with the Metropolis-Hastings algorithm. We employed two likelihood functions in our analysis: an “error-tolerant” likelihood function (see “a conservative formulation” by Sivia & Skilling 2006) given by

$$\prod_{i=1}^N \frac{1}{\sigma_w} \frac{1 - e^{-r_i^2/2}}{r_i^2} \quad (2)$$

and a least-squares likelihood function given by

$$- \prod_{i=1}^N \frac{1}{\sigma_w} e^{-r_i^2/2}, \quad (3)$$

where N is the number of measured H II regions. Note the factor $1/\sigma_w$ in the likelihoods, often a constant and ignored, is retained here since we vary its value in order to estimate arm width.

The error-tolerant likelihood function is relatively insensitive to outlying data points and was used to find and then remove interarm H II regions from the sample in an unbiased fashion. We accomplished this by fitting with the Equation (2) likelihood and discarding H II regions with $>3\sigma$ deviations. After this preliminary editing, we fitted the spiral with the least-squares likelihood (Equation (3)). Usually, at this stage, all residuals were $<3\sigma$, but occasionally one or two H II regions with

Table 2
NGC 628 (M74) Spiral Arm Segment Characteristics

| Arm | Azimuth Range (deg) | Mean Radius (kpc) | Pitch Angle (deg) | Width (kpc) |
|-----|-----------------------|-------------------|-------------------|-----------------|
| A | 90 \rightarrow 225 | 2.58 ± 0.02 | -27.6 ± 0.6 | 0.14 ± 0.02 |
| ... | 225 \rightarrow 310 | 5.60 ± 0.04 | -9.4 ± 1.0 | 0.34 ± 0.03 |
| ... | 310 \rightarrow 360 | 7.31 ± 0.06 | -18.1 ± 2.3 | 0.42 ± 0.04 |
| B | 50 \rightarrow 125 | 5.75 ± 0.04 | -15.2 ± 1.0 | 0.27 ± 0.03 |
| ... | 125 \rightarrow 195 | 7.57 ± 0.05 | -15.9 ± 1.1 | 0.46 ± 0.04 |
| ... | 195 \rightarrow 255 | 10.38 ± 0.08 | -11.0 ± 1.6 | 0.87 ± 0.06 |
| ... | 255 \rightarrow 290 | 12.02 ± 0.05 | -15.4 ± 1.2 | 0.59 ± 0.04 |

Notes. Arm segments are labeled with letters A and B and are defined by the indicated azimuth range. Azimuth increases east of north (counter clockwise from vertical in Figures 1 and 2). Mean radius is the fitted galactocentric distance at the average azimuth of the H II regions in the arm segment.

residuals just above 3σ were encountered. In these cases, the outliers were removed from the sample and the spiral re-fitted.

We first fitted a single log-periodic spiral to all H II regions in a given arm. Such “global” fits usually revealed systematic departures from a constant pitch angle model. Since we would like to investigate the possible increase in arm width along the arm, we re-fit each arm with spiral segments of length roughly 5–10 kpc. The boundaries for the arm segments were chosen based on three criteria: (1) breaks in the density or scatter of H II regions, (2) apparent changes in the local pitch angles among segments, and (3) to keep comparably sized samples of H II regions among the segments in one arm. Fitting short arm segments also has the advantage of minimizing systematic error in the width estimates, owing to the simplification of the assumed spiral model.

Marginalized posteriori probability density functions (PDFs) were obtained from binned histograms of the individual parameter values for all trials. Since the PDFs were approximately Gaussian in shape, we adopted the center and half-width of the 68% confidence intervals as best estimates of the parameter values and 1σ uncertainties.

4. RESULTS

4.1. NGC 628 (M74)

The image of NGC 628 (M74) is displayed in the left panel of Figure 1. This galaxy has two prominent spiral arms that wind counterclockwise with increasing distance from the galactic center. We could trace 223 H II regions in the arm labeled “A” in the figure and in Table 2 from a distance of about 2 to 8 kpc from the center. Fitting the log-periodic

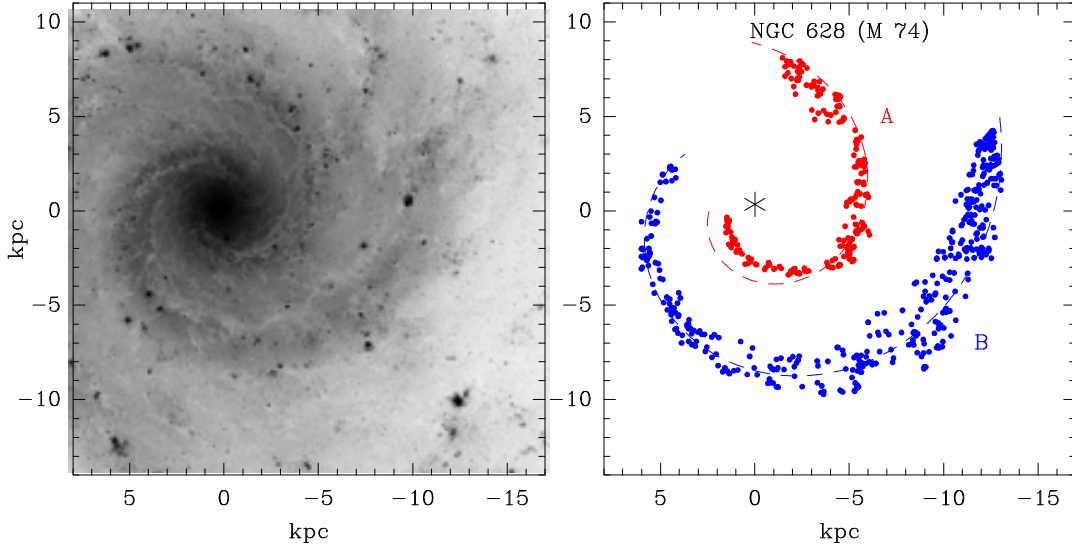


Figure 1. Left panel: image of NGC 628 (M74) in an $H\alpha$ filter with north up and east to the left. Right panel: locations of measured $H II$ regions. Dashed lines are a log-periodic spiral fitted to all $H II$ regions in arms labeled A and B, separately.

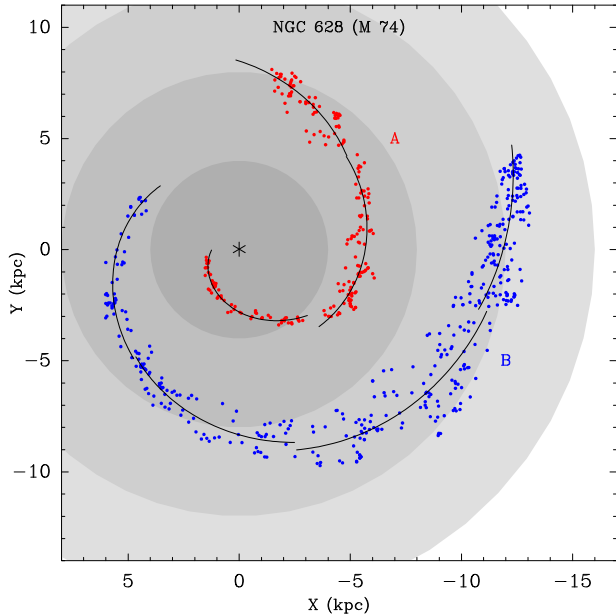


Figure 2. Locations of measured $H II$ regions for NGC 628 (M74) indicating the segments of each arm fitted with a spiral. Gray shaded annulae are spaced by 4 kpc and provide constant radius references. (The data used to create this figure are available.)

spiral form of Equation (1) to all $H II$ region positions gives a global pitch angle of -15.4 ± 0.5 , although it is clear that a single pitch angle is not a good fit over the entire arm. In the second arm, labeled “B,” we located 427 $H II$ regions between distances of about 4 to 13 kpc and find a global pitch angle of -14.3 ± 0.2 . This global fit is better than for arm A, but still shows some small systematic deviations from a constant pitch angle form.

We divided arm A into three segments and arm B into four segments, as indicated in Table 2. Spiral fits revealed significant changes in pitch angle among the segments in arm A, but only small changes among segments in arm B. For both arms, the

Table 3
NGC 1232 Spiral Arm Segment Characteristics

| Arm | Azimuth Range (deg) | Mean Radius (kpc) | Pitch Angle (deg) | Width (kpc) |
|-----|-----------------------|-------------------|-------------------|-----------------|
| A | $-45 \rightarrow 55$ | 3.33 ± 0.04 | -9.9 ± 1.5 | 0.16 ± 0.03 |
| ... | $45 \rightarrow 150$ | 5.01 ± 0.08 | -8.9 ± 2.3 | 0.52 ± 0.06 |
| ... | $150 \rightarrow 230$ | 5.98 ± 0.08 | -14.3 ± 2.1 | 0.51 ± 0.06 |
| B | $50 \rightarrow 165$ | 2.63 ± 0.03 | -11.8 ± 0.9 | 0.10 ± 0.02 |
| ... | $165 \rightarrow 250$ | 3.49 ± 0.04 | -10.8 ± 1.6 | 0.24 ± 0.03 |
| ... | $250 \rightarrow 315$ | 5.46 ± 0.06 | -26.6 ± 2.3 | 0.33 ± 0.04 |
| ... | $312 \rightarrow 380$ | 7.64 ± 0.07 | -30.0 ± 1.5 | 0.46 ± 0.04 |
| C | $-80 \rightarrow -20$ | 4.38 ± 0.03 | -14.7 ± 1.3 | 0.12 ± 0.02 |
| ... | $-20 \rightarrow +35$ | 5.82 ± 0.05 | -20.9 ± 1.2 | 0.27 ± 0.03 |
| D | $155 \rightarrow 195$ | 9.87 ± 0.04 | -10.9 ± 0.9 | 0.16 ± 0.03 |
| E | $-85 \rightarrow -65$ | 11.38 ± 0.05 | -11.6 ± 2.9 | 0.24 ± 0.04 |
| ... | $-65 \rightarrow -40$ | 12.83 ± 0.03 | -22.0 ± 1.0 | 0.14 ± 0.02 |
| F | $95 \rightarrow 130$ | 16.23 ± 0.10 | -10.8 ± 1.9 | 0.65 ± 0.07 |

Notes. Arm segments are labeled with letters A through F and are defined by the indicated azimuth range. Azimuth is measured east of north (counter clockwise from vertical in Figures 3 and 4).

estimated arm widths increase with increasing radius, with the exception of the last segment of arm B, where some narrowing occurs. These characteristics are evident from an inspection of Figure 2 where individual arm segment fits are displayed.

4.2. NGC 1232

The left panel of Figure 3 shows the image of NGC 1232, which displays several spiral arms starting from near the galactic center and winding counterclockwise with increasing radial distance. Some of these arms branch and/or connect with arm segments at large distances. We traced 105, 165, and 73 $H II$ regions in arms labeled “A” through “C,” respectively, and 25, 50, and 48 $H II$ regions in arm segments “D” through “F,” as labeled in the figure and in Table 3. Arm segments E and F may connect to spiral arms A and C, although other possibilities exist. Fitting a spiral form to all $H II$ regions in each arm

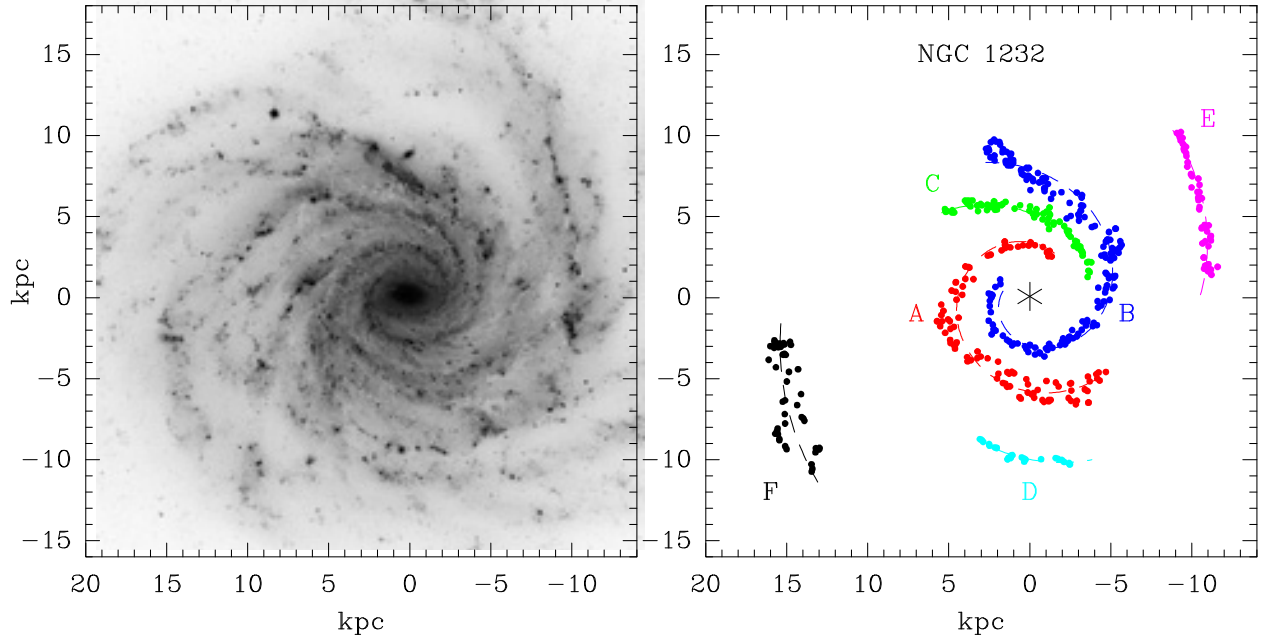


Figure 3. Left panel: image of NGC 1232 in blue filter. Right panel: locations of measured H II regions. Dashed lines are a log-periodic spiral fitted to all H II regions in arm segments A through F, separately.

Table 4
NGC 3184 Spiral Arm Segment Characteristics

| Arm | Azimuth Range (deg) | Mean Radius (kpc) | Pitch Angle (deg) | Width (kpc) |
|-----|---------------------|-------------------|-------------------|-----------------|
| A | 0 → 180 | 1.43 ± 0.04 | -22.8 ± 1.9 | 0.19 ± 0.03 |
| ... | 180 → 260 | 2.79 ± 0.07 | -14.9 ± 3.7 | 0.32 ± 0.05 |
| ... | 260 → 320 | 3.91 ± 0.08 | -22.7 ± 3.9 | 0.47 ± 0.05 |
| B | -180 → -130 | 1.09 ± 0.02 | -5.4 ± 1.2 | 0.07 ± 0.01 |
| ... | -30 → 45 | 2.57 ± 0.05 | -26.9 ± 2.5 | 0.24 ± 0.03 |
| ... | +45 → 120 | 3.95 ± 0.09 | -12.2 ± 3.3 | 0.42 ± 0.07 |

Notes. Arm segments are labeled with letters A and B and are defined by the indicated azimuth range. Azimuth increases east of north (counter clockwise from vertical in Figures 5 and 6).

(segment) gave global pitch angles of $-9^\circ 7 \pm 0^\circ 5$, $-17^\circ 3 \pm 0^\circ 4$, $-18^\circ 4 \pm 0^\circ 5$, $-10^\circ 9 \pm 0^\circ 9$, $-16^\circ 7 \pm 0^\circ 6$, and $-10^\circ 8 \pm 1^\circ 9$ for arms or segments A through F, respectively. Not only is a single pitch angle inappropriate for all arms, the longer arms clearly show systematic deviations from a constant pitch angle along their length.

We divided arms A, B, and C into two or more segments in order to estimate arm widths as a function of distance from the galactic center, as indicated in Table 3. The outer galaxy arm fragments D and F were fit with one segment and E with two segments. The spiral fits revealed significant changes in pitch angle among segments within arms. The widths for arms A, B, and C increase with distance from the galaxy center, as is evident in Figure 4. Only the outer galaxy arm segment E shows evidence arm narrowing.

4.3. NGC 3184

An image of NGC 3184 is displayed in the left panel of Figure 5. This galaxy has two prominent and symmetrical spiral arms that wind counterclockwise with increasing distance from

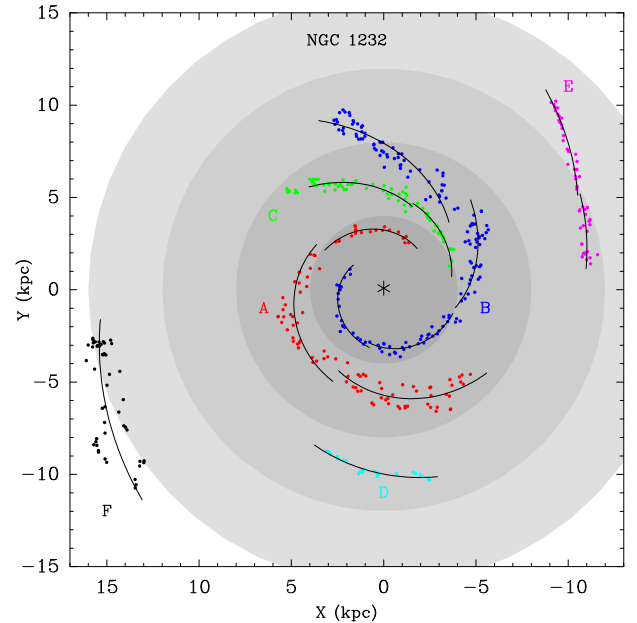


Figure 4. Locations of measured H II regions for NGC 1232 indicating the segments of each arm fitted with a spiral. Gray shaded annulae are spaced by 4 kpc and provide constant radius references. (The data used to create this figure are available.)

the galactic center. We could trace 100 and 80 H II regions in arms labeled “A” and “B,” respectively, in the figure and in Table 4, with distances of about 1 to 5 kpc from the center. Fitting spirals to all H II region positions for arms A and B separately gives global pitch angles of $-19^\circ 6 \pm 0^\circ 6$ and $-20^\circ 2 \pm 0^\circ 8$. These values are consistent with each other.

We divided arms A and B into three segments each, as indicated in Table 4. The spiral fits revealed significant changes

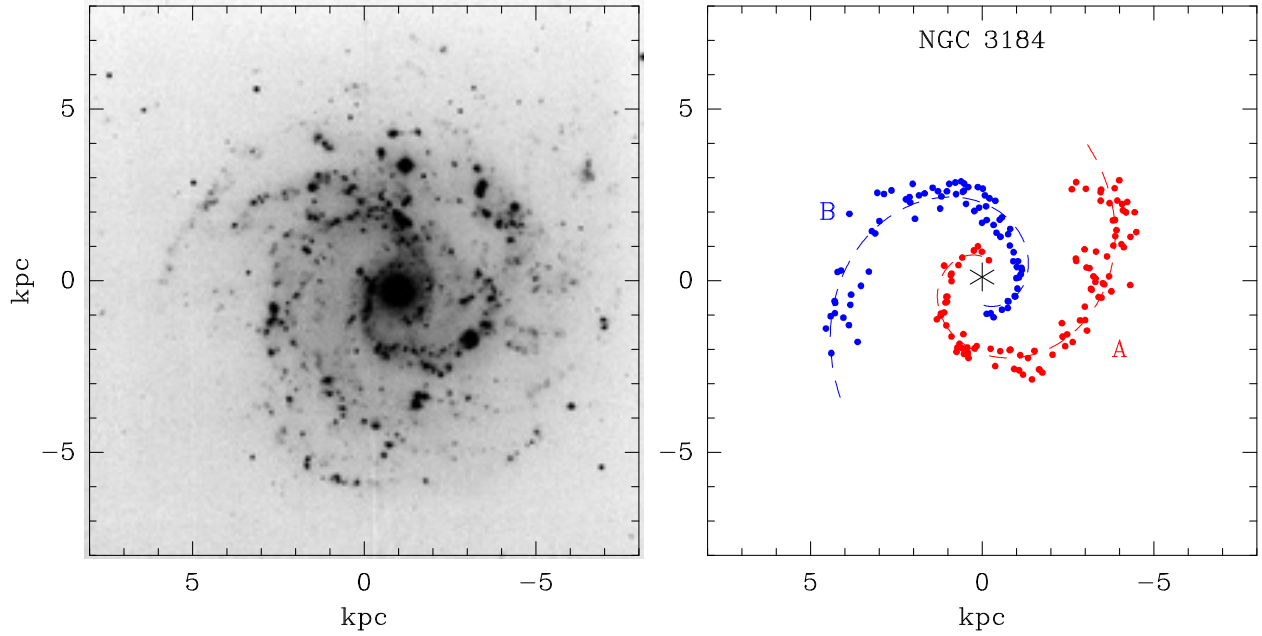


Figure 5. Left panel: image of NGC 3184 in an H α filter. Right panel: locations of measured H II regions. Dashed lines are a log-periodic spiral fitted to all H II regions arms labeled A and B, separately.

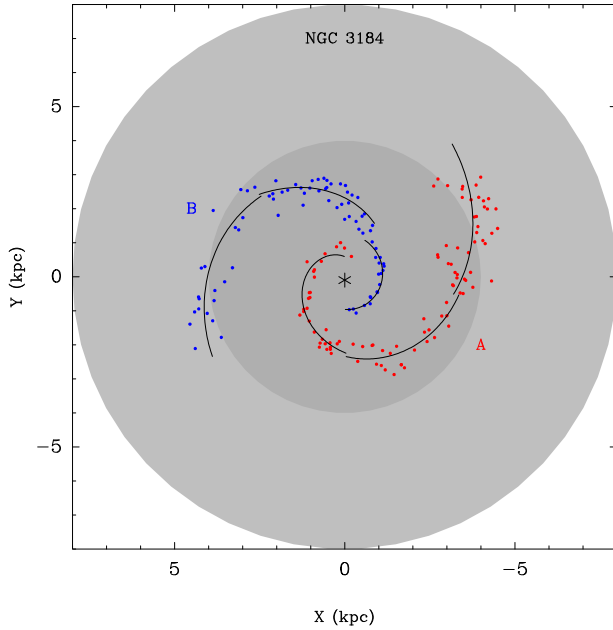


Figure 6. Locations of measured H II regions for NGC 3184 indicating the segments of each arm fitted with a spiral. Gray shaded annulae are spaced by 4 kpc and provide constant radius references. (The data used to create this figure are available.)

in pitch angle among segments within each arm. The widths for both arms increase smoothly with distance from the galaxy center, as is evident in Figure 6.

4.4. NGC 5194 (M51)

The image of NGC 5194 is displayed in the left panel of Figure 7. This galaxy has two prominent spiral arms that wind

Table 5
NGC 5194 (M51) Spiral Arm Segment Characteristics

| Arm | Azimuth Range (deg) | Mean Radius (kpc) | Pitch Angle (deg) | Width (kpc) |
|-----|-------------------------|-------------------|-------------------|-----------------|
| A | 250 \rightarrow 170 | 1.90 ± 0.02 | $+30.9 \pm 0.7$ | 0.07 ± 0.01 |
| ... | 165 \rightarrow 80 | 3.29 ± 0.02 | $+15.0 \pm 0.9$ | 0.18 ± 0.02 |
| ... | 80 \rightarrow 30 | 5.40 ± 0.04 | $+26.7 \pm 1.7$ | 0.26 ± 0.02 |
| ... | 30 \rightarrow -15 | 6.45 ± 0.04 | -9.1 ± 2.0 | 0.31 ± 0.03 |
| ... | -15 \rightarrow -40 | 6.08 ± 0.04 | -4.0 ± 4.7 | 0.23 ± 0.03 |
| B | 65 \rightarrow -40 | 2.50 ± 0.03 | $+22.5 \pm 1.1$ | 0.14 ± 0.02 |
| ... | -40 \rightarrow -90 | 3.42 ± 0.04 | $+1.2 \pm 2.6$ | 0.20 ± 0.03 |
| ... | -90 \rightarrow -150 | 5.39 ± 0.03 | $+19.4 \pm 1.0$ | 0.28 ± 0.02 |
| ... | -150 \rightarrow -200 | 6.70 ± 0.05 | $+8.6 \pm 1.6$ | 0.37 ± 0.03 |
| ... | -200 \rightarrow -250 | 7.11 ± 0.05 | -10.3 ± 1.4 | 0.43 ± 0.04 |
| ... | -250 \rightarrow -305 | 7.05 ± 0.04 | $+19.2 \pm 1.3$ | 0.46 ± 0.03 |
| ... | -305 \rightarrow -345 | 9.72 ± 0.05 | $+28.9 \pm 2.0$ | 0.22 ± 0.03 |

Notes. Arm segments are labeled with letters A and B and are defined by the indicated azimuth range. Azimuth increases east of north (counter clockwise from vertical in Figures 7 and 8).

clockwise with increasing distance from the galactic center. We could trace 283 and 527 H II regions in arms labeled “A” and “B,” respectively, in the figure and in Table 5, with distances of about 2 to >10 kpc from the center for arm B. Fitting spirals to all H II region positions for arms A and B separately gives global pitch angles of $+13.4 \pm 0.6$ and $+8.3 \pm 0.3$, which are significantly different. While systematic deviations from the global model for arm A are modest, those for arm B are large.

We divided arms A and B into five and six segments, respectively, as indicated in Table 5. The spiral fits revealed significant changes in pitch angle among segments with each arm. Overall, the widths for both arms increase smoothly with distance from the galaxy center, as is evident in Figure 8. However, both show a narrowing in their last segment.

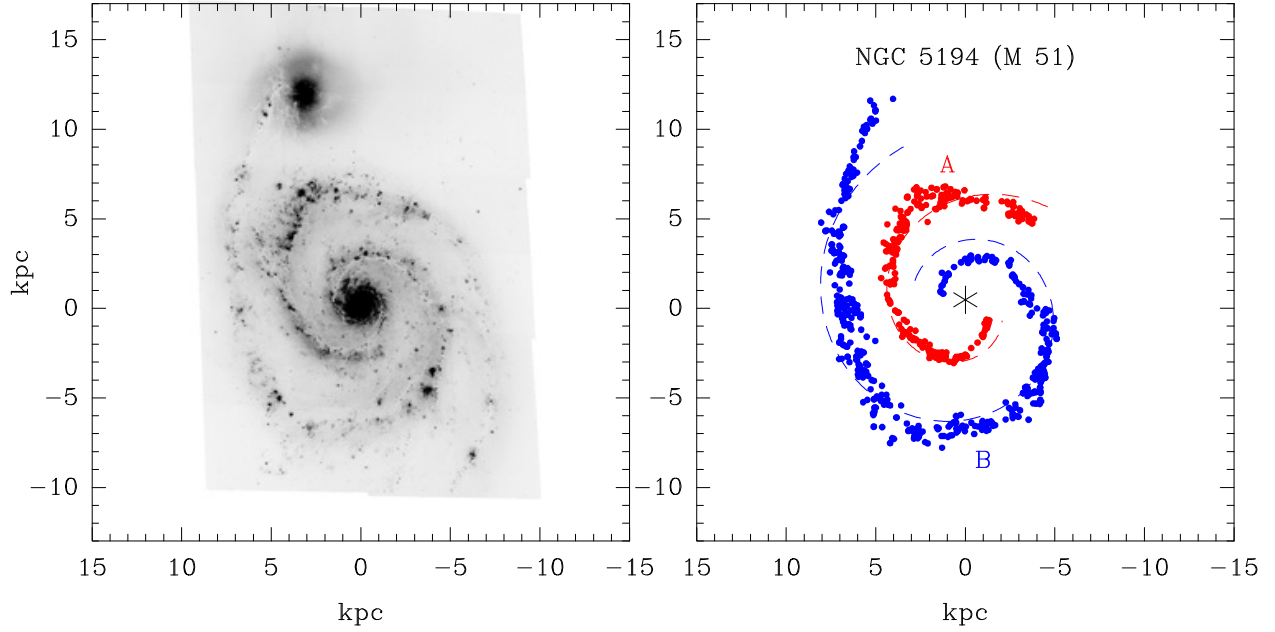


Figure 7. Left panel: image of NGC 5194 (M51) in H α filter. Right panel: locations of measured H II regions.

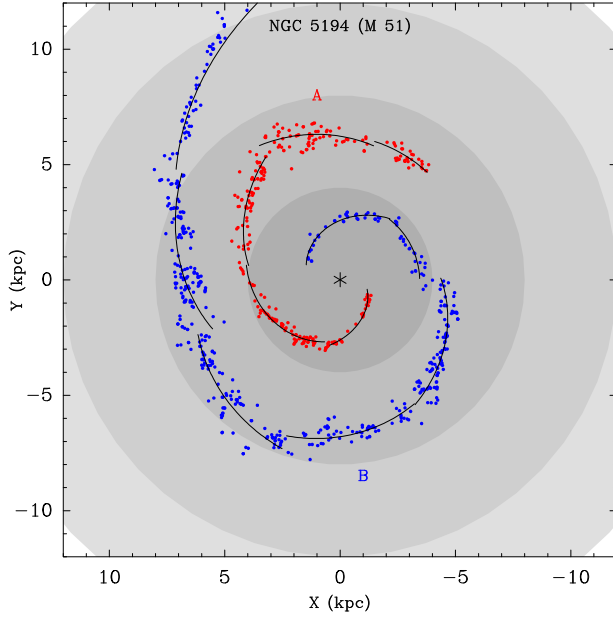


Figure 8. Locations of measured H II regions for NGC 5194 (M51) indicating the segments of each arm fitted with a spiral. Gray shaded annulae are spaced by 4 kpc and provide constant radius references.
(The data used to create this figure are available.)

5. CHARACTERISTICS OF SPIRAL ARMS

Many studies present the properties of spiral arm pitch angles averaged over an entire galaxy (e.g., Kennicutt 1981; Savchenko & Reshetnikov 2013; Davis & Hayes 2014). Often these use Fourier or other automated techniques that can efficiently analyze large samples of galaxies using integrated light. Our work differs by directly fitting spirals to the locations of H II regions, which allows a detailed and robust evaluation

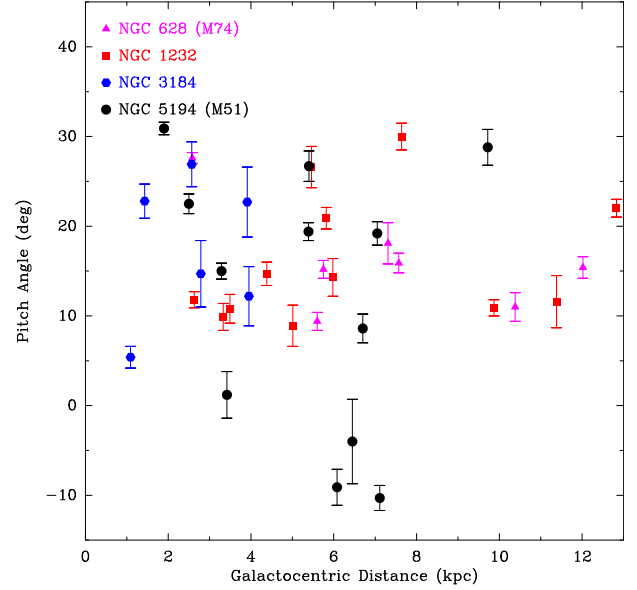


Figure 9. Pitch angles of spiral arms segments vs. galactocentric distance for four galaxies measured in this work. Galaxy identifiers and plotting symbols are indicated in the upper left of the figure. For the three galaxies that wind counter-clockwise outward from the galactic center, we have plotted the negative of the measured values. There is a large scatter in pitch angles both among arms in different galaxies, among arms within a galaxy, and even along a single spiral arm.

of the characteristics of spiral arms without assuming uniform properties over an entire arm or galaxy.

5.1. Pitch Angles

Figure 9 shows the measured pitch angles of the segments of spiral arms in our sample of galaxies. Most pitch angles for these galaxies are between about 10° and 30°, comparable to the range found by Kennicutt (1981) for Sc-type galaxies.

Note that we also find large variations of pitch angles among arms within a spiral galaxy, as well as along individual arms, confirming previous studies (e.g., Russell & Roberts 1992; Ma 2001; Savchenko & Reshetnikov 2013; Davis & Hayes 2014).

Interestingly, we find no evidence for a general change in pitch angle with galactocentric distance. The N -body simulations of Grand et al. (2013) suggest that the pitch angle of an arm segment decreases with the local rate of shear in a galaxy's rotation, and that shear rate generally increases with radius. Thus, one might expect a small trend of pitch angle decreasing with galactocentric radius. However, they also find that arm segments are short-lived and change pitch angles by $\sim 10^\circ$ over time scales of ~ 0.1 Gyr. This may explain the apparent random variation in pitch angles within each galaxy in our sample, since different arm segments would likely be observed at different ages.

The characteristics of pitch angles of Milky Way spiral arms are now being revealed by trigonometric parallax measurements of high-mass star forming regions from observations with the Very Long Baseline Array, the Japanese VERA project, and the European VLBI Network. Using parallax results from these arrays yielded pitch angle estimates for sections of the following Milky Way arms: Scutum arm: $\psi = 19.8 \pm 3.1$ (Sato et al. 2014), Sagittarius arm: $\psi = 7.3 \pm 1.5$ (Wu et al. 2014), Local arm: $\psi = 10.1 \pm 2.7$ (Xu et al. 2013), Perseus arm: $\psi = 9.7 \pm 1.5$ (Zhang et al. 2013; Choi et al. 2014), and Outer arm: $\psi = 14.9 \pm 2.7$ (Hachisuka et al. 2015). The variation of pitch angle among segments of Milky Way spiral arms is qualitatively similar to those of the four late-type spirals in this study. Currently the parallax data for the Milky Way typically trace only arm segments ~ 5 to 10 kpc in length, which corresponds to the scale over which we find relatively constant pitch angles in the external galaxies. However, as larger regions of the Milky Way are mapped, one might expect to see pitch angle variations along its spiral arms.

5.2. Arm Widths

Figure 10 shows the widths of arm segments (defined as the scatter perpendicular to the arm of their H II regions) for the four galaxies in our sample. Only arms with two or more fitted segments are plotted. Except for the three outliers in the lower-right portion of the figure, which indicate narrowing at the ends of some arms (to be discussed below), both individually and as a group these data indicate that spiral arms increase in width with distance from the center of their galaxy. Clear examples of this phenomenon are seen in Figure 2 for arm B of NGC 628 (M74) and in Figure 6 for arm A of NGC 3184. Lynds (1970) reported a similar result for the widths of primary dust lanes associated with spiral arms.

Unlike spiral pitch angles that vary significantly and randomly across a galaxy, the widths of arm segments display a systematic variation with radius. Thus, the observed arm-width versus radius trends should provide a clear observable to test and better understand N -body simulations. At present we are unaware of arm width estimates from simulations.

A similar analysis by Reid et al. (2014) for Milky Way spiral arms noted that the scatter in H II regions, based on trigonometric parallax distances, increased with distance from the Galactic center. This result motivated us to examine external spiral galaxies to determine if the Milky Way is typical or unusual in this respect. Although based on this relatively small sample of external galaxies, we conclude that spiral arms widths in the Milky Way are qualitatively similar to those in other spiral galaxies.

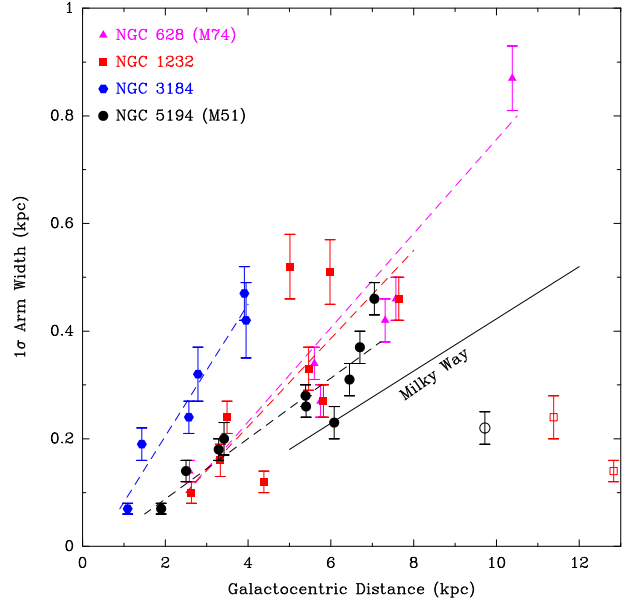


Figure 10. Widths of spiral arms vs. galactocentric distance for four galaxies. Galaxy identifiers and plotting symbols are indicated in the upper left of the figure. Only arms with two or more fitted segments are plotted. Open symbols indicate outermost arm distances if narrowing is observed. Dashed lines indicate trends for each galaxy. The solid line is arm-width vs. radius for the Milky Way, based on trigonometric parallax distances for high-mass star forming regions (Reid et al. 2014).

Interestingly, in NGC 628 (M74) arm B, NGC 1232 arm E, and NGC 5194 (M51) arms A and B, we find that the trend of arm width increasing with distance reverses near the outer tips of these arms. These last arm segments are all significantly narrower than their immediately interior arm segment. This narrowing appears related to massive star formation dying out at large galactocentric radii. In classical spiral density-wave theory, this narrowing could be attributed to reaching the radius of co-rotation of a spiral pattern with orbiting material. If so, M51's arm A co-rotates at a radius of ≈ 6 kpc while arm B co-rotates at a radius of ≈ 9 kpc. The existence of (at least) two co-rotation radii in M51 would argue against a single (global) pattern speed, consistent with the findings of Meidt et al. (2008).

5.3. Spiral Arm Formation

The trend of spiral arm width increasing with galactocentric distance demonstrated in this paper may provide a diagnostic characteristic for constraining models of the origin of spiral arms. The swing amplification mechanism (Goldreich & Lynden-Bell 1965) may lead to such a trend, as swinging inherently fans material outward (Toomre 1981). Whether or not global spiral density-wave theories naturally lead to the observed growth of arm width has not been addressed.

In the galaxies we studied, a small number of spiral arms display nearly continuous arms with modest changes in pitch angle. However, more commonly, we find the arms are much less regular. Examination of Figures 2, 4, 6, and 8 reveals that individual arms often break up into segments of ~ 5 kpc length, and different segments join to form bends, kinks, and quasi-linear sections and abrupt changes in pitch angle. Similar conclusions have been reached based on a variety of other observables (e.g., Russell & Roberts 1992; Waller et al. 1997; Chernin 1999). To these characteristics we now add variation in

arm width. These observations suggest that spiral arms are not purely global structures.

Numerical simulations of galactic disks also show spiral characteristics that indicate non-global origin (e.g., Foyle et al. 2011; Grand et al. 2012). In particular, the high-resolution N -body simulations by D’Onghia et al. (2013) show that spiral structures can form in response to perturbations from giant molecular clouds in the disk, which then swing amplify to form arm segments, grow non-linearly, and then connect to produce long spiral-like patterns. Given the arm morphologies we have noted in late-type galaxies, such an origin for spiral arms seems an attractive mechanism.

We thank the referee and E. D’Onghia for suggestions to improve the paper.

REFERENCES

- Chernin, A. D. 1999, *MNRAS*, **308**, 321
- Choi, Y. K., Hachisuka, K., Reid, M. J., et al. 2014, *ApJ*, **790**, 99
- Davis, D. R., & Hayes, W. B. 2014, *ApJ*, **790**, 87
- D’Onghia, E., Vogelsberger, M., & Hernquist, L. 2013, *ApJ*, **766**, 34
- Foyle, K., Rix, H.-W., Dobbs, C. L., Leroy, A. K., & Walter, F. 2011, *ApJ*, **735**, 101
- Goldreich, P., & Lynden-Bell, D. 1965, *MNRAS*, **130**, 125
- Grand, R. J. J., Kawata, D., & Cropper, M. 2012, *MNRAS*, **421**, 1529
- Grand, R. J. J., Kawata, D., & Cropper, M. 2013, *A&A*, **553**, A77
- Hachisuka, K., Choi, Y. K., Reid, M. J., et al. 2015, *ApJ*, in press
- Kennicutt, R. C., Jr. 1981, *AJ*, **86**, 1847
- Knapen, J. H., Stedman, S., Bramich, D. M., Folkes, S. L., & Bradley, T. R. 2004, *A&A*, **426**, 1135
- Lynds, B. T. 1970, in IAU Symp. 38, The Spiral Structure of our Galaxy, ed. W. Becker & G. I. Kontopoulos (Dordrecht: Reidel), 26
- Ma, J. 2001, *ChJAA*, **1**, 395
- Meidt, S. E., Rand, R. J., Merrifield, M. R., Shetty, R., & Vogel, S. N. 2008, *ApJ*, **688**, 224
- Reid, M. H., Menten, K. M., Brunthaler, A., et al. 2014, *ApJ*, **783**, 130
- Russell, W. S., & Roberts, W. W., Jr. 1992, *ApJ*, **398**, 94
- Sato, M., Wu, Y. W., Immer, K., et al. 2014, *ApJ*, **793**, 72
- Savchenko, S. S., & Reshetnikov, V. P. 2013, *MNRAS*, **436**, 1074
- Sivia, D., & Skilling, J. 2006, *Data Analysis: A Bayesian Tutorial* (2nd ed.; New York: Oxford Univ. Press), 168
- Toomre, A. 1981, in *Structure and Evolution of Normal Galaxies*, ed. S. M. Fall & D. Lynden-Bell (Cambridge: Cambridge Univ. Press), 111
- Waller, W. H., Bohlin, R. C., Cornett, R. H., et al. 1997, *ApJ*, **481**, 169
- Wu, Y. W., Sato, M., Reid, M. J., et al. 2014, *A&A*, **566**, 17
- Xu, Y., Li, J. J., Reid, M. J., et al. 2013, *ApJ*, **769**, 15
- Zhang, B., Reid, M. J., Menten, K. M., et al. 2013, *ApJ*, **775**, 79